Camera Dynamic Range Measurement: The Role of Lenses and Target Spatial Distribution

Alice Plutino, Michele Bagnati, and Alessandro Rizzi

***Abstract*— High dynamic range (HDR) is still considered a technological issue related to sensors' dynamic or effectiveness of multiple exposures. To this aim, test charts have been devised to supposedly measure this sensor/camera limit. This study aims to show how these test charts do not measure the actual camera dynamic range (DR) since this depends on the spatial arrangement and size of test chart luminance values and on the chosen lens. In this work, we have reported test measures that show how camera DR acquisition depends on the scene spatial distribution of luminance and the glare caused by lens optical scattering. We have reported measures that underline how glare (or flare) represents the main DR limitation in the acquisition phase of systems with lenses, and we assess its influence on the DR of the acquired image. The experiments performed in this work were done in a controlled environment, and pointwise instrumental measures were compared with camera acquisitions using different lenses and setups. The tests here presented report a reduction in the acquired DR of 48% on average, varying across different test setups, with four different lens types and five step chart layers forming varying DRs. Here, we propose a more realistic point of view in DR assessment since the effect of glare and spatial distribution of luminances in the acquired DR is massive, systematic, and unavoidable.**

***Index Terms*— Dynamic range (DR), flare, glare, glare measurement, imaging.**

I. Introduction

THE dynamic range (DR) is defined as the ratio between the maximum and minimum luminance in the observed scene, which depends on the emitted and reflected light intensity in the scene. In digital imaging, DR can also be defined with measures related to how light intensity is digitized and quantized and it is considered a technological issue related to sensors' dynamic or effectiveness of multiple exposures [1], [2].

In this article, we do not deal with these aspects since our interest is what happens to light before it is captured by the sensor.

The need to acquire and handle a wide DR has various fields of application, ranging from artistic to scientific [3], [4]. Today, the film industry is working more and more frantically to reduce risks and time waste while acquiring or editing high DR (HDR) images and videos for several applications.

To achieve this article's aim, we first need to introduce an important optical phenomenon: glare.

A. Glare

There is a potential language ambiguity between the two terms Glare and Flare. Both refer to the role of optics, but in some fields of research and applications, one term is used to indicate a sort of quasiuniform loss of contrast in the whole image, while the other refers to the local distortions caused by highlights. Here, we want to underline that there is no advantage in differentiating these two aspects that originate from the same optical effect. For this reason, we will use the term glare to refer univocally to the same optical phenomenon.

Glare is an unavoidable optical phenomenon that takes place in the lenses when photographing or filming a scene. It causes a loss of contrast, resulting in a reduction of the acquired DR. In many cases, the glare effect (GE) results in invisibleness since our vision system compensates for it, while in some cases, it can be identified as a veil, flashes, or rays of light in various directions. Glare is caused by the scattering of light in the camera lenses, thus affecting all the imaging systems with lenses (see Figs. 1 and 2). In general, the more complex the optics structure, the greater the departure of the acquired values from the actual ones in the scene. High-quality lens coatings can reduce this effect, but not significantly. Glare is systematically unavoidable [4], [8], [9], [10]. More in detail, glare is defined by ISO as the percentage of light that scatters from a point source. This underlines an important property: glare is independent of light intensity. Following this principle, the veiling glare index (VGI) is defined as the ratio of the irradiance at a specified position along the centerline of the image of a narrow, perfectly black band superimposed on an extended field of uniform radiance to the irradiance at the same point of the image plane when the black band is removed. VGI is expressed as a percentage unless otherwise specified [11]. The spatial figure of glare is a circular symmetric spread function that depends on the material crossed by the light ray (see Fig. 1).

Glare dominates DR measurements and strongly depends on the spatial arrangement of luminances in the scene; it follows that different test charts (and, consequently, the actual scene) can result in different acquired DRs. Test chart designs have different density patterns and, thus, different amounts of glare (see Fig. 2). Generally, the larger the bright (white/transparent) areas, the greater the glare and the lower the measured DR [3], [12]. A commonly used target reference is the Xyla diagram

Manuscript received 28 January 2024; revised 2 April 2024; accepted 17 April 2024. Date of publication 13 May 2024; date of current version 28 May 2024. This work was supported by the European Union's Horizon Research and Innovation Program through Marie Skłodowska-Curie Actions (MSCA) Postdoctoral Fellowships 2022 (HORIZON-MSCA-2022-PF-01) under Agreement 101105533. The Associate Editor coordinating the review process was Dr. Jingtao Sun. *(Corresponding author: Alice Plutino.)*

Alice Plutino is with the Media Studies Department, University of Amsterdam, 1012 WP Amsterdam, The Netherlands (e-mail: a.plutino@uva.nl).

Michele Bagnati and Alessandro Rizzi are with the Computer Science Department, Università degli Studi di Milano, 20122 Milan, Italy.

Digital Object Identifier 10.1109/TIM.2024.3400303

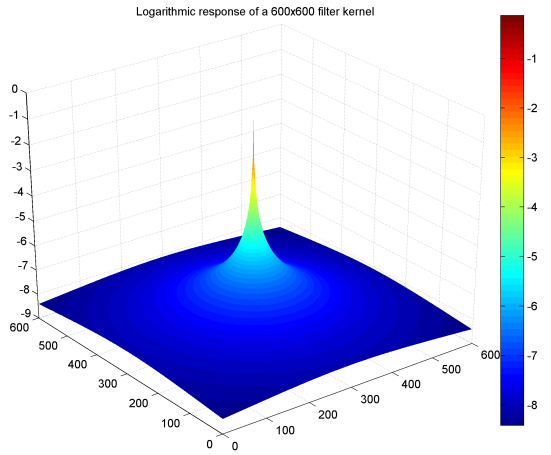

Fig. 1. Spatial figure of glare (i.e., glare spread function). The plot is derived from a kernel of size 600 × 600. See the source code [5] derived from [6] and [7].

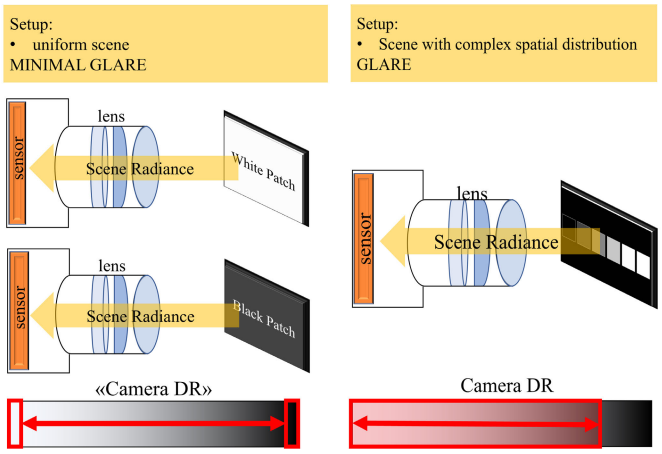

Fig. 2. Graphical representation of two camera DR assessment setups. In the first case (left), DR is measured through two acquisitions: one of a uniform white patch and one of a uniform black patch. In this case, DR is minimally affected by lens glare. In the second case (right), DR is measured through the acquisition of a stepchart (i.e., DR target) arranged in a more complex scene. In this case, DR is lowered by lens glare enhanced by the scene context.

produced by DSC Labs [13]. These targets can be of three types Xyla16, Xyla21, and Xyla26, which claim to offer 15, 20, and 25 stops of DR. They have become an international standard for measuring the DR of camera systems (ISO 15739:2017).

B. DR Definition and Measurement

The main contribution of this article is to move from a theoretical idea of DR acquisition to consider real limits, in particular, the most important one, the optic glare, that is usually misconsidered in the major part of the article that deals with the problem of DR acquisition correctness (see literature reported in this section).

DR can be measured at many steps of the acquisition pipeline, as presented in Fig. 3. DR originates from the light of the scene and ends with light displayed by the monitor, passing through digits that, in the theoretical premises, should represent specific amounts of light.

A widely considered parameter to assess the DR of an imaging system is sensor sensitivity, thus the range of brightness

TABLE I
STANDARD SENSOR DR AND DR MEASUREMENTS

Measure	Standard	Main Formula	Reference
Sensor DR	EMVA 1288	$DR = \frac{\mu_{p.sat}}{\mu_{p.min}}$ $\mu_{p.sat}$: saturation irradiation; $\mu_{p.min}$: absolute sensitivity threshold.	[20]
DR	ISO 15739:2013	$DR = \frac{L_{sat}}{L_{min}}$ L_{sat}: the saturation luminance; L_{min}: luminance where SNR = 1.	[18]

between sensor saturation and a fixed value of signal-to-noise ratio. It is usually measured in RAW images and in a sequence of flat field exposures (often involving calibrated neutral density filters), for example, using the EMVA 1288 standard [14], [15] (see Table I). Sensor manufacturers are developing HDR image sensors that claim exceptional DRs (120 dB to as much as 150 dB). Still, the system's measured DR is typically much lower than the specified sensor DR [16], which is caused primarily by the glare of the system lenses [17].

The calculation of DR according to ISO 15739:2013, revised in 2017 and 2023 [18], provides an estimation based on a patch with a density of 2.0, commonly found on semi-gloss reflective test charts (see Table I) [19]. This approach relies on chart values, like the tests presented in this work. The results presented in this article prove that the test charts are not representative of the high variability of real scenes for which the system's performance can vary a lot.

II. EXPERIMENTAL SETUP

The above-presented standard approaches are usually confused with "whole-system" measures since they do not consider glare, a major limit for the acquired DR.

From the presented overview, we can assess that even if glare is a known phenomenon, since it is scene-dependent, many DR metrics and measurements do not consider it, and DR assessment is performed just at the sensor level. This approach can cause misunderstandings and incorrect evaluations, especially in cameras and systems that use different lenses on the same body. In this work, we aim to perform a DR evaluation using a simple stepchart, constant setup, and expositions to assess the role of lenses in DR systems. More specifically, we focus on glare assessment and measurement, varying optics and scene DR, with specific attention on optics setups, without including acquisition parameters like image formats or gamma curves from which glare is independent.

The final aim of this study is to raise attention to glare, an unwanted and systematic phenomenon that strongly interacts with DR assessments and must be considered when developing new metrics and imaging systems. The tests and experiments designed in this work aim to underline that DR can only be measured relatively, according to the spatial arrangement of the target chosen, and that this does not represent an absolute DR limit of the system.

To run these tests, we have designed a target able to cover a very high DR and then we have used it to assess the limit of digital acquisition. The experiments were conducted in a dark room without windows and natural light sources.

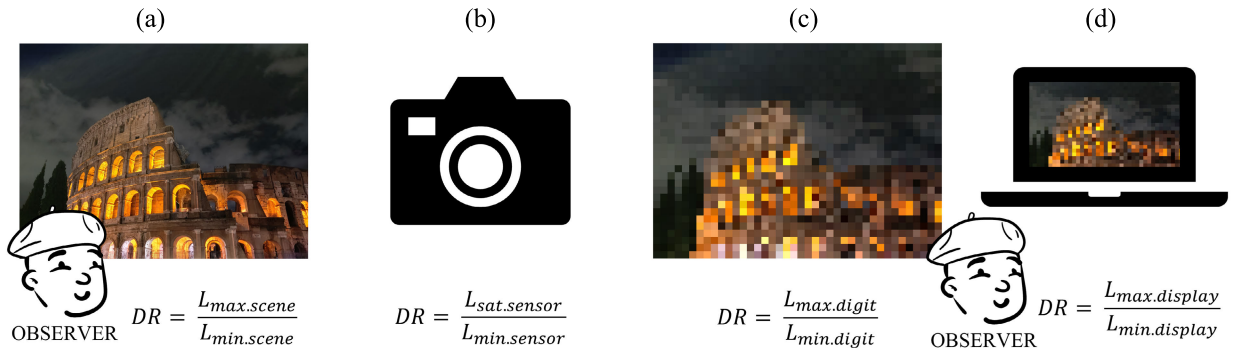

Fig. 3. Graphical description of DR computation. (a) Real scene. (b) Acquisition. (c) Digital data. (d) Display.

A. Diffused Light Source

We designed and devised a diffuse light source called a cloud light box (CLB) to perform the experiments. LED sources are a good solution owing to their capacity to mitigate excessive energy consumption while upholding elevated brightness levels. For the experiment reported here, parameters like correlated color temperature (CCT) and color rendering index (CRI) have not been considered since the targets are black and white. Attention has been paid to heat dissipation, working voltage, and maximum current. In this context, controlling and monitoring voltage fluctuations is fundamental, whether they are continuous or alternating. LEDs solely emit light under positive voltage conditions. Any deviations in voltage over time will correspondingly alter the luminous output. Changes in input voltage can result in flickering issues.

For this reason, we used a dc stable voltage (not switching) as a CLB power supply to avoid flickering problems. Furthermore, since a common problem with light sources is overheating, which can damage the LEDs, to avoid overheating we used a current limiter (present in the power supply circuit) and foresight to prevent prolonged work periods.

Considering the diffused light source's requirements, the CLB comprises 70-W COB LED panels with a significant emission and dissipation surface. Each panel has a maximum operating voltage of 14 V and a limiting current of 6000 mA. The emission surface is 203 × 100 mm. Operating in direct voltage allows for varying the light emitted, allowing for a very versatile CLB. The three panels can be power supplied both in series and in parallel. The parallel mode would have involved a very high current, reaching 18 A. In this case, current limiting would have been costly and the voltage inaccurate, given that the operating range is from 9.5 to 14 V. The three LED panels have been connected in series with a Boost Converter to limit the current easily and have a broader voltage regulation.

We have added a digital multimeter in series to monitor volt and ampere values. In the case of the CLB, the voltage and current values used are 2 A and 34 V, respectively. The LEDs and the power supply module are subject to overheating, so providing a better heat dissipation system for prolonged use or with high voltages is necessary. In our experiment, 5 min of inactivity is enough to bring the system back to a temperature close to the ambient temperature.

To increase light diffusion, we have used a box internally painted in matte white, with a front panel and a completely matte black exterior paint. The frontal panel has a 3-mm-thick opaque white polycarbonate panel, which is relatively rigid and transparent. The panel diffuses the light uniformly, and the measurements made by isolating various emission areas show maximum differences of ±0.1 EV.

A representation of the CLB is reported in Fig. 4(a)–(c) (images obtained using Fusion360, software from the Autodesk suite).

B. Stepchart Patches

Five identical grayscale diagrams have been designed with GIMP and printed on transparent paper using a laser printer. To obtain a high contrast in the scene and thus enter the HDR area, single transparency is not enough for darkening, so in the test, we overlapped up to five grayscale transparencies (five layers). During the tests, the layers have been directly superimposed using a customized mask to avoid displacements. The measures were performed by shooting with each camera setup and adding a new layer after the captures. The patches used in the experiment are gray squares visible in Fig. 5.

Each backlit patch has been measured with a Konica Minolta CL 70F illuminance meter, covering all the other patches with black cardboard during the measures (see Section II-D1).

For the imaging acquisitions, transparencies were fixed on the polycarbonate panel (see Fig. 6) and acquired using a camera with different lenses. The camera used is a Canon 800D [21] with an APS-C sensor that captures raw images (CR2 extension). We used a tripod and remote control in the experiment to avoid vibrations during acquisition and speed up the process. All automatic camera settings have been disabled and manually fixed. The autofocus of the lenses was deactivated immediately after focusing on the scene.

In the presented experiments, two terms will be used to easily distinguish the data within the tests: Measured, Data collected with the illuminance meter CL70; Acquired, Data collected through the camera.

C. Test Procedure and Lenses

All the images have been acquired using the exposure bracketing technique to use only the linear portion of the

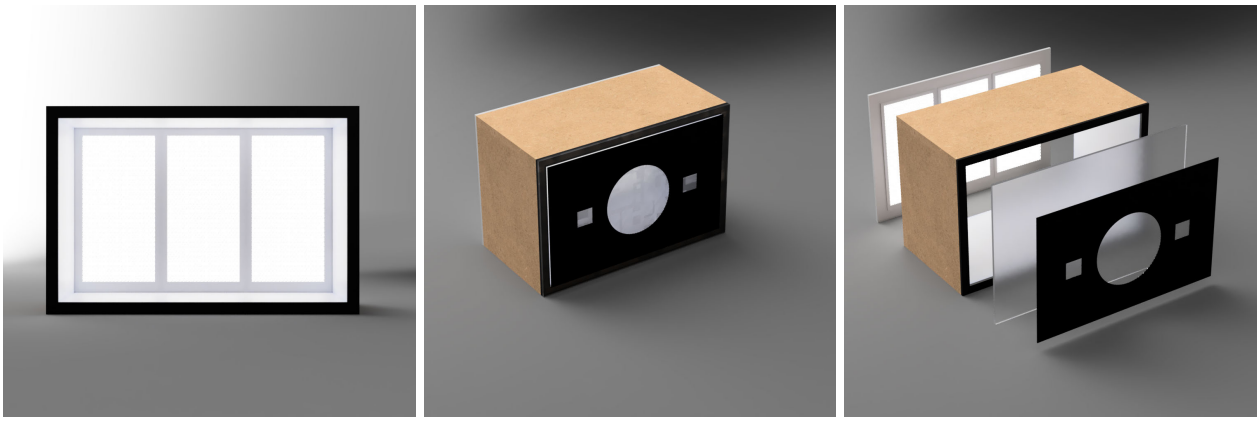

(a) (b) (c)

Fig. 4. (a)–(c) CLB simulation in Fusion360.

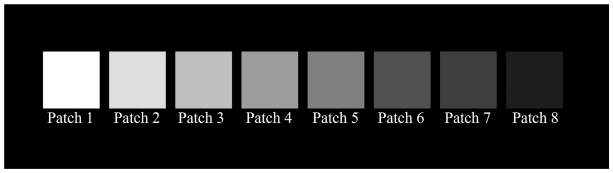

Fig. 5. Eight patches with different gray values.

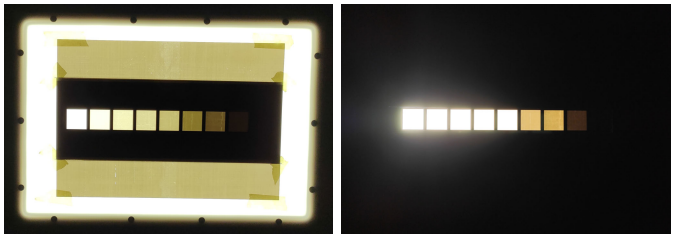

Fig. 6. On the left, an example of transparency is placed on the CLB. On the right is an example of an image acquisition setup.

TABLE II

CAMERA OPTICS USED IN THE EXPERIMENT

ID	Lens name	Glass/Group
A	Canon EF-S 24mm f/2.8 STM	6/5
B	Sigma 18-35mm f/1.8 DC HSM Art	17/12
C	Sigma 17-50mm f/2.8 EX DC OS HSM	17/13
D	Sigma 50-150mm f/2.8 EX DC OS HSM APO	21/15

sensor curve without incurring noise or saturation problems (see Section II-D2).

The optics used in the experiment are 4, all with Canon EF bayonet. To facilitate the reading of the data, a letter has been associated with each one (see Table II).

D. Glare Measurement

Glare is a scene- and system-dependent scattered light falling on image sensors. It limits the range of acquired luminances; thus, the DR. Glare or flare is defined in the standard ISO 9358:1994 (reviewed and confirmed in 2019) [11], and two different measurements are reported: the VGI and the glare spread function. In the ISO standard, glare is described as generated from the sum of individual light contributions to a single pixel from all the light sources from the scene, which is scattered by the lens surfaces and camera walls, causing an unwanted light diffusion on the sensor. In ISO 9358:1994, the glare spread function quantifies the stray light relative to the angle from an intense, small light source. Veiling glare is calculated as the proportion of light scattered from a large white background into a central opaque spot. The report provides standards for comparing different lenses and apertures.

ISO 9358:1994 presents several limits. It applies solely to optical systems (lenses), excluding the influence of image sensors and camera image processing, it mandates stricter testing conditions and it lacks a grayscale step chart for tonal response measurement in images [22], [23], [24]. Because of that, the ISO 18844:2017 has been developed.

ISO 18844:2017 veiling glare is measured from charts that contain black holes in a larger white field. Also, in this case, many limits have been underlined, in fact, it only characterizes short-range glare, without providing information on long-range glare [25], and ignores the effect of the glare spread function [26].

The ISO standard glare measurement methods present some limits of application, thus we measured this effect using chart-based measurements and compared the illuminance values of measured and acquired data.

Following the glare effect (GE) measure proposed in [17], we computed the glare of the imaging system as:

$$\mathrm{GE} = \frac{\mathrm{rv}_l^p}{\mathrm{RV}_l^p} \tag{1}$$

where rv_l^p is the ratio between the acquired value in patch p, and the acquired white value in the same layer l. RV_l^p is the ratio between the measured transmitted light in patch p and the measured light in the white patch of the same layer l

$$\mathrm{RV}_l^p = \frac{L_l^p}{L_l^w} \tag{2}$$

where L_l^p corresponds to the illuminance of patch p in layer l, and L_l^w to the illuminance of the white patch w, in the same layer l (e.g., $\mathrm{RV}_5^8 = (4.2/44200) = 0.0001$; see Table III and Fig. 7).

This measure allows us to assess the difference in ratio between the measured and acquired patches to define the amount of glare that causes the DR reduction in the acquisitions. Different lenses and setups will help us assess the main parameters contributing to the overall glare amount.

TABLE III
PATCHES ILLUMINANCE VALUES (LUX) MEASURED WITH THE CL70F AT DIFFERENT LAYERS

Lux	1 Layer	2 Layers	3 Layers	4 Layers	5 Layers
Patch1	55900	53500	48500	41800	44200
Patch2	48700	39000	30100	24700	20000
Patch3	41600	28600	18700	13900	10200
Patch4	34700	20200	12100	6740	4220
Patch5	27600	13500	6260	3020	1670
Patch6	17200	5670	1810	600	222
Patch7	12900	3220	847	227	65.5
Patch8	7080	1020	155	23.6	4.2

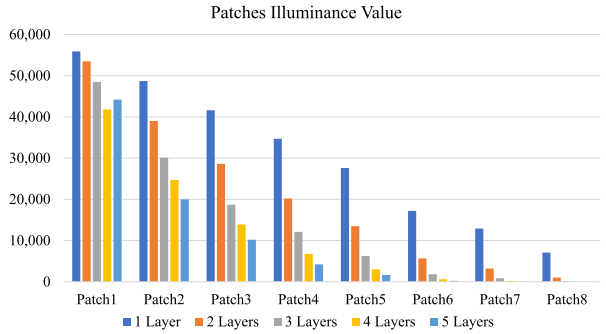

Fig. 7. Graphical representation of the patches illuminance values measured in lux (see data from Table III).

1) Measured Data: Table III presents measures of each patch of the stepchart (CL70F).

2) Acquired Data: Data acquisitions with the camera have been made using different parameters of focal length and sensor distance from the light source. More specifically, the optics A, B, and C have a focal length of 24 mm and have been used at a distance from the CLB of 57 mm. Lens D has a focal length of 150 mm and has been used at 245 mm from the target.

Images have been acquired using the bracketing technique. Bracketing (i.e., exposure bracketing) is a photographic method used to ensure optimal exposure in challenging lighting conditions or when uncertainty exists about the correct exposure settings. It involves taking multiple shots of the same scene at varying exposure levels, typically adjusting the aperture, shutter speed, or ISO settings between shots. In this work, all the setups from 1 to 5 layers have been acquired for each lens using a shutter speed from 1/4000 to 30 (1 EV increment), keeping constant the ISO and aperture (f 5.6).

After acquiring the images (in total 360), we extracted the raw values of the pixels inside each patch using LibRaw [27]. In this work, we considered as digits the average RGGB values in a 240 × 240-pixel area from the patch center.

According to the technical specifications, the camera has a measurement range of EV from 1 to 20. So, we measured the camera's characteristic curve setting up a scene at 6 EV (measured with a Konica Minolta Spotmeter F). In this case, the acquired scene has been created by placing an LED light source behind a matte Plexiglass panel in a uniform diffused light scene (6 EV in the whole acquisition frame). In this setup, the camera measured 0 EV using lens A (Canon EF-S 24 mm), f 8, ISO 100, and with a shutter speed of 0.6 s. To correlate the camera digit with the illuminance and plot the camera's characteristic curve, we extracted the digit from a central area

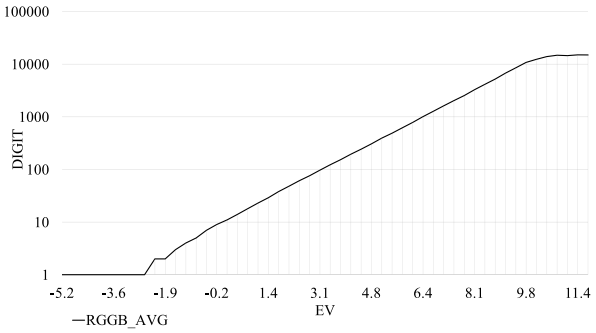

Fig. 8. Camera sensor curve obtained from the digit and lux values in a scene of EV 6. The average values of RGGB are reported here.

of 64 × 64 pixels. The camera's characteristic curve is reported in Fig. 8. The measurement of the camera's characteristic curve and the application of the bracketing technique make it possible to work with multiple-exposure images, thus selecting the digit values acquired using the sensor's linear portion for each setup. In fact, if in one layer and two layers, a shutter speed of 1/500 was sufficient to correctly acquire all the patches in the scene without background noise or saturation, in setups with higher DR, it was necessary to join the values of at least two acquisitions at different exposures. Furthermore, thanks to the assessment of the camera's characteristic curve, it is possible to correlate the acquired digit values with the illuminance measurements. Data are reported in Table IV and plotted in Figs. 9 and 10.

As for the measured data, to assess the overall GE [see (1)], we computed rv_l^p as

$$\mathrm{rv}_l^p = \frac{D_l^p}{D_l^w} \tag{3}$$

where D_l^p is the average digit value of patch p in layer l, and D_l^w is the average digit value of the white patch w in the same layer l. For example, using lens A, $\mathrm{rv}_5^8 = (1.10/4549) = 0.0002$ (see Table IV).

III. RESULTS AND DISCUSSION

To assess and measure the influence of glare in systems DR, we compared the images' acquired values with the measured luminance values.

A. GE Measurements

As a first analysis of the results, we computed the GE [see (1)] between the measured and acquired patches using different lenses (A, B, C, and D), from 1 to 5 layers. The GE values and results are reported in Table V and Fig. 11.

The GE using one, two, and three layers is quite negligible; the black patch (patch 8) presents slight variations.

With four layers, patch 8 has a GE from 1.93 to 2.20 depending on the lens (see Table V). In this case, the best-performing lens is the 150 mm Sigma (D).

Considering five layers, we have measured values of GE from 2.48 to 3.75 in patch 8 (see Table V).

In Fig. 11, we plotted the values of GE in three different patches (patches 2, 5, and 8) at different layers for each considered lens (A, B, C, and D). Here, it is possible to see the

TABLE IV

DIGIT ACQUIRED VALUES OF THE EIGHT PATCHES AT DIFFERENT ACQUISITION SETUPS (A, B, C, AND D), USING FROM 1 TO 5 LAYERS. SEE THE GRAPHICAL VISUALIZATION IN FIGS. 9(C) AND 10

1 Layer								
digit	Patch1	Patch2	Patch3	Patch4	Patch5	Patch6	Patch7	Patch8
A	5674	5331	4929	4382	3704	2534	1934	1135
B	5904	5521	5068	4510	3806	2596	1989	1168
C	4992	4701	4353	3876	3274	2242	1713	1002
D	5343	4936	4492	3973	3337	2287	1764	1053
2 Layers								
digit	Patch1	Patch2	Patch3	Patch4	Patch5	Patch6	Patch7	Patch8
A	5432	4495	3647	2769	1915	887	526	185
B	5236	4316	3483	2647	1829	844	504	177
C	4749	3942	3206	2431	1687	844	463	163
D	5078	4142	3307	2491	1713	792	475	170
3 Layers								
digit	Patch1	Patch2	Patch3	Patch4	Patch5	Patch6	Patch7	Patch8
A	5294.50	3837.50	2727.50	1771.00	876.13	328.75	148.44	30.94
B	5134	3700	2620	1708	978	323.94	146.94	31.19
C	4556	3312	2364	1543	887	293.81	132.75	28.06
D	4860	3469	2427	1571	890	292	134	28.44
4 Layers								
digit	Patch1	Patch2	Patch3	Patch4	Patch5	Patch6	Patch7	Patch8
A	4712	2999	1892	1061	511	109	42.69	5.34
B	4480	2834	1781	997	529.38	109.13	38.88	5.56
C	4289	2735	1730	973	468	106.97	38	5.25
D	4594	2887	1786	997	510.75	105.31	37.50	5
4 Layers								
digit	Patch1	Patch2	Patch3	Patch4	Patch5	Patch6	Patch7	Patch8
A	4549	2539	1407	680	275	39	12.28	1.10
B	4556	2517	1387	672	271	41.39	11.89	1.63
C	3975	2218	1232	597	266.50	37.31	10.69	1.38
D	4242	2328	1275	606	265.31	37.06	10.38	1

TABLE V

GE IN THE EIGHT PATCHES USING DIFFERENT ACQUISITION SETUPS (A, B, C, AND D). SEE THE GRAPHICAL VISUALIZATION IN FIG. 11

1 Layer								
	Patch1	Patch2	Patch3	Patch4	Patch5	Patch6	Patch7	Patch8
GE A	1.00	1.08	1.17	1.24	1.32	1.45	1.48	1.58
GE B	1.00	1.07	1.15	1.23	1.31	1.43	1.46	1.56
GE C	1.00	1.08	1.17	1.25	1.33	1.46	1.49	1.58
GE D	1.00	1.06	1.13	1.20	1.26	1.39	1.43	1.56
2 Layers								
	Patch1	Patch2	Patch3	Patch4	Patch5	Patch6	Patch7	Patch8
GE A	1.00	1.14	1.26	1.35	1.40	1.54	1.61	1.79
GE B	1.00	1.13	1.24	1.34	1.38	1.52	1.60	1.77
GE C	1.00	1.14	1.26	1.36	1.41	1.68	1.62	1.80
GE D	1.00	1.12	1.22	1.30	1.34	1.47	1.55	1.76
3 Layers								
	Patch1	Patch2	Patch3	Patch4	Patch5	Patch6	Patch7	Patch8
GE A	1.00	1.17	1.34	1.34	1.28	1.66	1.61	1.83
GE B	1.00	1.16	1.32	1.33	1.48	1.69	1.64	1.90
GE C	1.00	1.17	1.35	1.36	1.51	1.73	1.67	1.93
GE D	1.00	1.15	1.30	1.30	1.42	1.61	1.58	1.83
4 Layers								
	Patch1	Patch2	Patch3	Patch4	Patch5	Patch6	Patch7	Patch8
GE A	1.00	1.08	1.21	1.40	1.50	1.61	1.67	2.01
GE B	1.00	1.07	1.20	1.38	1.64	1.70	1.60	2.20
GE C	1.00	1.08	1.21	1.41	1.51	1.74	1.63	2.17
GE D	1.00	1.06	1.17	1.35	1.54	1.60	1.50	1.93
5 Layers								
	Patch1	Patch2	Patch3	Patch4	Patch5	Patch6	Patch7	Patch8
GE A	1.00	1.23	1.34	1.57	1.60	1.71	1.82	2.54
GE B	1.00	1.22	1.32	1.54	1.57	1.81	1.76	3.75
GE C	1.00	1.23	1.34	1.57	1.77	1.87	1.81	3.64
GE D	1.00	1.21	1.30	1.50	1.66	1.74	1.65	2.48

increase of GE graphically, mainly in the darkest patch (patch 8), together with the GE variation caused by using different lenses. This evidences a strong influence of glare increasing the black patch brightness and underlines the big difference in the subsequent assessment of DR considering just the sensor or the whole system (see Section III-C).

B. Further Investigation: Are Glare Targets Equivalent?

A further investigation was done on another test with four layers overlapped, this time with two lines of gray patches, one bright to dark (A Up) and the other dark to bright (A Down) [see Fig. 12(a)]. In Table VI are reported the digit values obtained in this setup.

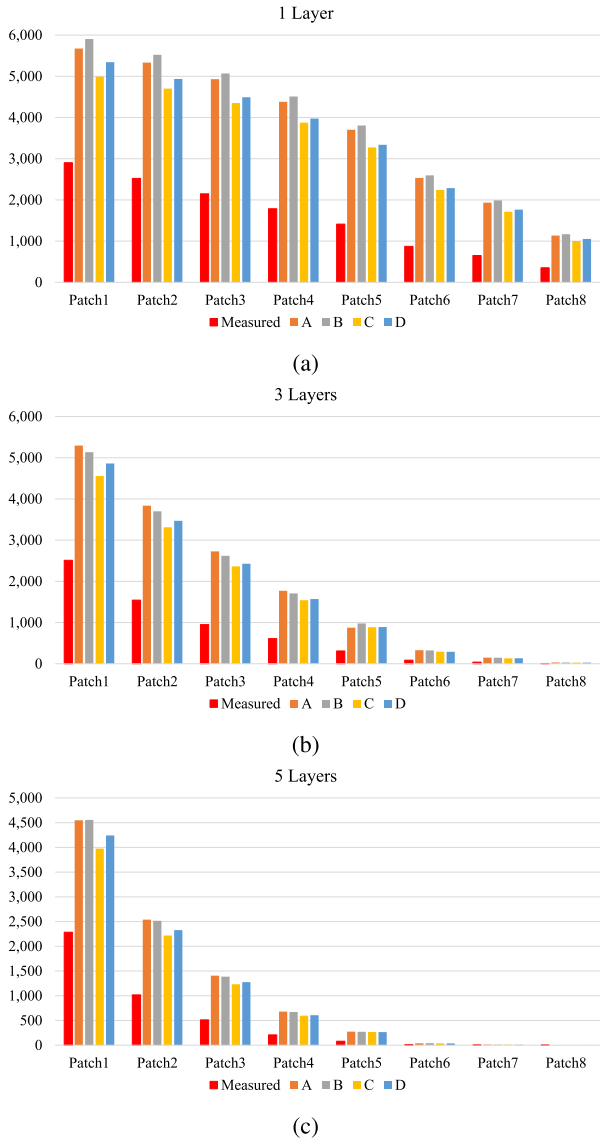

Fig. 9. Graphical representation of the measured and acquired values of the eight patches at different acquisition setups (A, B, C, and D) using 1 Layer (a), 3 Layers (b), and 5 Layers (c). The measured values in lux have been converted into digits through the camera's sensor curve. See Fig. 10 for a more detailed visualization of the values of patch 8.

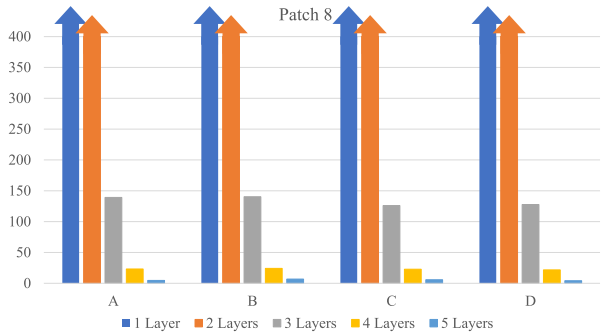

Fig. 10. Graphical representation of the digit values of patch 8 to make them more readable.

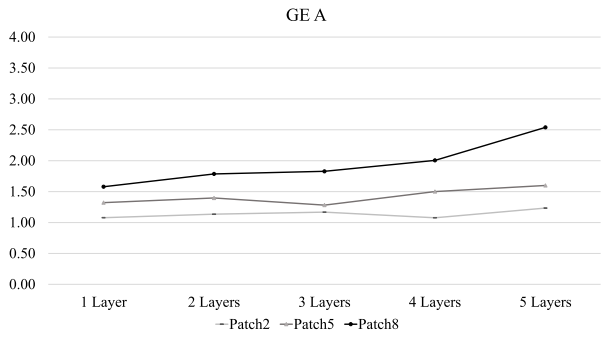

(a)

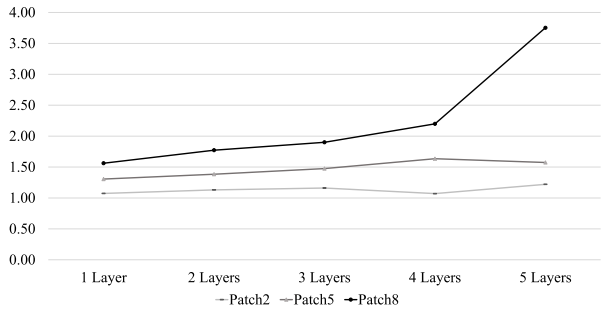

(b)

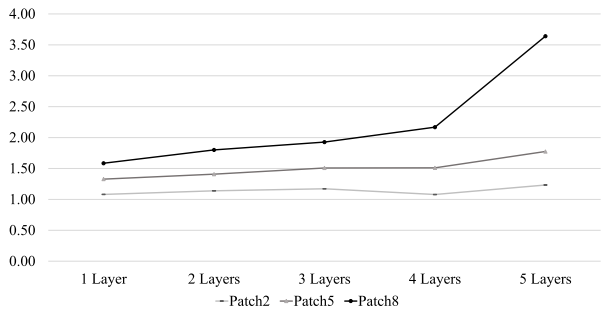

(c)

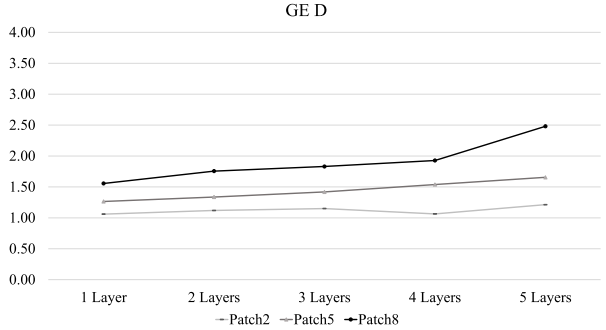

(d)

Fig. 11. GE in patches 2, 5, and 8, considering acquisitions using lens A (a), lens B (b), lens C (c), and lens D (d) at different layers.

Also in this case, to assess the glaring amount, we computed the GE [see (1)]. This further experiment assesses how much glare is generated by the scene setup and, thus by the scene's spatial arrangement. In Fig. 12(b) are plotted the values of GE in this setup, and in Table VII are reported the GE values of this setup and in Fig. 12(b) these values are plotted.

TABLE VI

DIGIT ACQUIRED VALUES OF THE 8 (UP) + 8 (DOWN) PATCHES USING LENS A AND FOUR LAYERS

4 Layers, two stepcharts								
Digit	Patch1	Patch2	Patch3	Patch4	Patch5	Patch6	Patch7	Patch8
Up	9449	6200	3924	2175	1053	220	79	10.38
Down	8979	6066	3948	2236	1094	218	84.75	10.63

TABLE VII

GE VALUES IN THE TWO (UP AND DOWN) STEPCHART SETUP (LENS A, FOUR LAYERS), COMPARED WITH THE GE OF ONE STEPCHART SETUP

4 Layers, two stepcharts								
	Patch1	Patch2	Patch3	Patch4	Patch5	Patch6	Patch7	Patch8
GE A	1.00	1.08	1.21	1.40	1.50	1.61	1.67	2.01
GE Up	1.00	1.11	1.25	1.43	1.54	1.62	1.54	1.94
GE Down	1.00	1.14	1.32	1.54	1.69	1.69	1.74	2.10

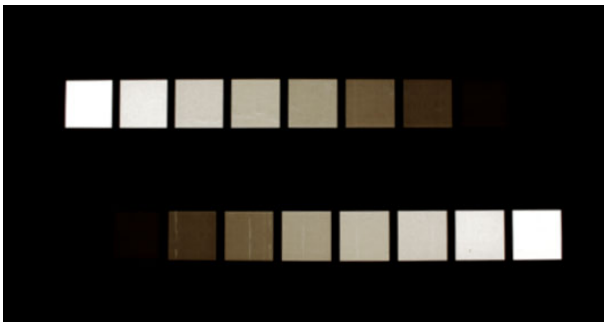

(a)

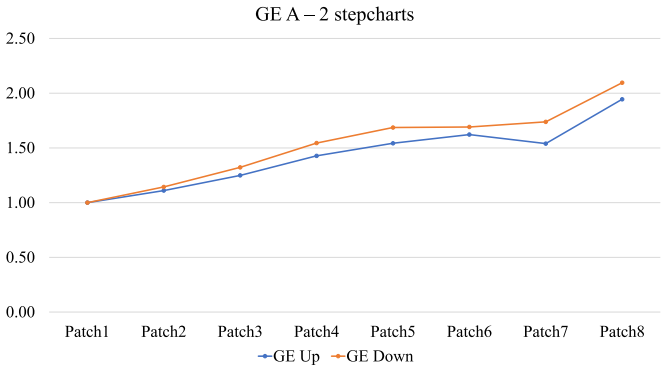

(b)

Fig. 12. (a) Example image of the two stepcharts analyzed in this experiment (A Up and A Down). (b) Plot of GE values acquired using lens A, two lines of gray patches (one up and one down) and four layers.

Considering this setup, the glare caused by the lightest patches strongly affects the dark surround and all the other patches in the scene, causing an increase in GE if compared with the data of the single stepchart in the same condition (see Table V). Here, it is possible to see that the chart setup influences the GE, which changes from a value of 2.01 (patch 8, lens A, four-layer setup) to 1.94 and 2.10 when two stepcharts are in the same scene. This GE increase is determined by the influence of the white patch (patch 1) and the light gray patches on the darkest patches, of which patch 8 (black) is the most affected.

C. DR Assessment

From the data acquired in the different testing sessions, we can assess the different settings measured (meas) and

TABLE VIII

SCENE SETUP DR_{MEAS} AND DR_{ACQ} USING DIFFERENT SETUPS A, B, C, AND D. SEE THE ABSOLUTE ERROR REPRESENTATION IN FIG. 13

	1 Layer	2 Layers	3 Layers	4 Layers	5 Layers
DR_{meas}	7.90	52.45	312.90	1771.19	10523.81
DR_{acq} A	5.00	29.36	171.14	883.07	4144.28
DR_{acq} B	5.05	29.58	164.62	805.39	2803.69
DR_{acq} C	4.98	29.13	162.35	816.95	2890.91
DR_{acq} D	5.07	29.87	170.90	918.80	4242.00

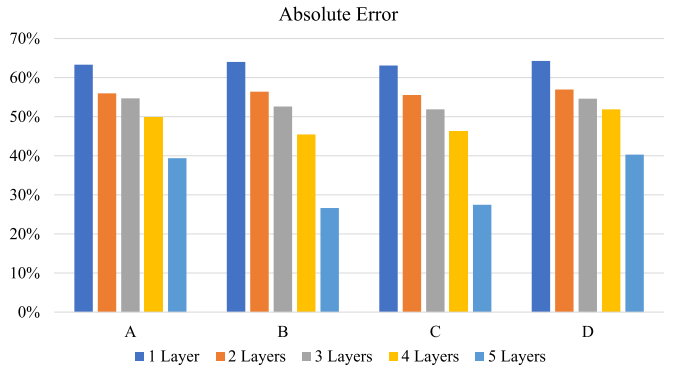

Fig. 13. Graphical representation of the absolute error of DR in percentage using different setups (A, B, C, and D) at different layers.

acquired (acq) DR. To measure the scene DR, we computed

$$\mathrm{DR}_{\mathrm{meas}} = \frac{L_i^w}{L_i^b} \tag{4}$$

and

$$\mathrm{DR}_{\mathrm{acq}} = \frac{D_i^w}{D_i^b}. \tag{5}$$

Data are reported in Table VIII and the absolute error representation is shown in Fig. 13.

Considering the differences between $\mathrm{DR}_{\mathrm{meas}}$ and $\mathrm{DR}_{\mathrm{acq}}$, it is clearly visible how the acquired DR always differs from the actual one. In no case was the camera able to acquire the real distribution of light. In the case of small DR (one or two layers), this difference is small and tends to get bigger while DR increases. In the worst case (five layers), the acquired DR is much less than half of the actual one as visible from Fig. 13.

This assessment underlines the influence of DR evaluation of the scene setup, thus the scene context and the system optics.

IV. DISCUSSION AND CONCLUSION

In this work, we have explored the role of lenses and target spatial distribution in camera DR acquisition assessment, reporting the heavy influence of optical glare in the reduction of acquired DR. In general, we can convey that camera DR acquisition depends on, in order of importance.

1) The scene spatial distribution of luminance.
2) The lenses.
3) The camera sensor.

The main contribution of this article is presenting numerically the impact of the first two parameters, while in many research and methodologies, popular in the field, DR measure typically relies solely on data from the camera sensor, disregarding the DR reduction caused by the entire optical system and the scene setup. Notably, glare emerges as a significant factor causing important DR reduction, leading to a significative loss of contrast.

Independent of sensors and scene exposure, glare causes an unwanted systematic deviation from actual scene values, significantly affecting the acquired image, especially in uncontrolled conditions.

Following these considerations, any possible test target for DR measure cannot be absolute. It can only measure the DR reduced by the target's precise spatial configuration of patch distribution and sizes. A different target with different types of patches and spatial distribution will report a different DR assessment.

In our research, we conducted various DR assessment tests to evaluate the influence of glare using different camera lenses and scene setups. While glare influence is noticeable even in scenes with low DR (up to 11 EV), its effect becomes more pronounced in higher DR scenarios (from 14 to 17 EV), where it can cause a reduction of up to 4 EV in DR, independently of the lens employed.

Through these tests and analyses, it becomes evident that the scene context holds paramount importance in DR acquisitions, followed by the optical system and the sensor. Consequently, it would be erroneous to define the DR of a system solely based on the sensor, without considering the spatial arrangement of the scene being captured and the contrast reduction of the lens scattering.

The outcomes of this research are generalizable to any possible lens type or configuration. As demonstrated by McCann and Rizzi [10], glare imposes limitations on DR both in digital and film cameras. Even in the case of lensless pinhole camera acquisition, the actual DR is affected by other optical issues, for example, diffraction, that make the acquired DR also, in this case, different from the actual one.

The glare measurement metric outlined by Signoroni et al. [17], utilized in our study, can be effectively employed across diverse scene arrangements and DR test charts, whether reference patches are present and contact luminance measurements can be performed.

In comparison with many other reports of DR assessment, here we demonstrate how something well-known in photographic optics must be considered since it significantly affects the acquired DR. Glare is intrinsic to any lens, making it impossible to test every lens comprehensively. The proposed measure is the acquired/scene DR values, and there is no need for any additional parameter to quantify DR reduction in the acquisition phase.

The complexity of glare assessment highlights a fundamental challenge in the field of imaging. While lens design and manufacturing techniques continually evolve, the idea of eliminating glare entirely remains an elusive goal. Therefore, the task of characterizing and mitigating glare falls upon researchers and practitioners. Our study underlines the importance of incorporating glare considerations into the DR evaluation, urging a paradigm shift in how we approach DR imaging. By acknowledging the systematic and unavoidable nature of glare, researchers can develop strategies to minimize

its impact, optimize image quality, and improve imaging models.

Looking to the future, it is important to recognize that the challenge posed by glare is more of a cultural one. Glare will never be entirely eliminable. The challenge now lies in cultural awareness, while we await future techniques that may help us estimate or reduce the effect of glare. Works on DR must start considering its existence, especially those aiming for some form of measurement from the scene. With this work, we hope to stimulate research to develop more prosperous and complex metrics and measurements to assess DR and link it to the assessment of glare in imaging systems.

REFERENCES

[1] A. R. Varkonyi-Koczy, A. Rovid, and T. Hashimoto, "Gradient-based synthesized multiple exposure time color HDR image," *IEEE Trans. Instrum. Meas.*, vol. 57, no. 8, pp. 1779–1785, Aug. 2008.

[2] M. Jiang, L. Shen, M. Hu, P. An, Y. Gu, and F. Ren, "Quantitative measurement of perceptual attributes and artifacts for tone-mapped HDR display," *IEEE Trans. Instrum. Meas.*, vol. 71, pp. 1–11, 2022.

[3] F. Dufaux, P. Le Callet, R. Mantiuk, and M. Mrak, *High Dynamic Range Video From Acquisition to Display and Applications*. New York, NY, USA: Academic, Apr. 2016.

[4] J. J. McCann and A. Rizzi, *The Art and Science of HDR Imaging*, vol. 26. Hoboken, NJ, USA: Wiley, 2011.

[5] V. Vonikakis, *Retinal-Contrast-Glare*. San Francisco, CA, USA: GitHub, 2022.

[6] J. J. McCann and V. Vonikakis, "Calculating retinal contrast from scene content: A program," *Frontiers Psychol.*, vol. 8, Jan. 2018, Art. no. 287438.

[7] J. J. McCann, V. Vonikakis, and A. Rizzi, "Edges and gradients in lightness illusions: Role of optical veiling glare," *Frontiers Psychol.*, vol. 13, Dec. 2022, Art. no. 958787.

[8] A. Rizzi and J. McCann, "Glare-limited appearances in HDR images," *J. Soc. Inf. Display*, vol. 17, no. 1, pp. 3–12, 2009.

[9] A. Silzars, A. Rizzi, and J. McCann, "Glare-limited appearances in HDR images," *Inf. Display*, vol. 25, p. 31, Jan. 2009.

[10] J. McCann and A. Rizzi, "Camera and visual veiling glare in HDR images," *J. Soc. Inf. Display*, vol. 15, pp. 721–730, Sep. 2007.

[11] *Optics and Optical Instruments Veiling Glare of Image Forming Systems Definitions and Methods of Measurement*, document ISO, & ISO 9358, 1994.

[12] A. Chalmers, P. Campisi, P. Shirley, and I. Olaizola, *High Dynamic Range Video, Concepts, Technologies, and Applications*. Hoboken, NJ, USA: Wiley, Apr. 2016.

[13] *Xyla*, Dsclabs, Mississauga, ON, Canada, 2015.

[14] M. Rosenberger, C. Zhang, P. Votyakov, M. Preißler, R. Celestre, and G. Notni, "EMVA 1288 camera characterisation and the influences of radiometric camera characteristics on geometric measurements," *Acta Imeko*, vol. 5, no. 4, pp. 81–87, 2016.

[15] B. Jähne, "Evaluation of modern image sensors using the EMVA 1288 standard," *Imag. Appl. Opt. Opt. Soc. Amer. Tech. Dig.*, vol. 2, pp. 1–32, Jul. 2016.

[16] *Dynamic Range*, ImaTest, Boulder, CO, USA, 2023. Accessed: Feb. 16, 2023.

[17] A. Signoroni, M. Conte, A. Plutino, and A. Rizzi, "Spatial–spectral evidence of glare influence on hyperspectral acquisitions," *Sensors*, vol. 20, no. 16, p. 4374, 2020.

[18] *Photography Electronic Still-Picture Imaging Noise Measurements*, document ISO 15739:2023, 2023.

[19] V.-T. Peltoketo, "Signal to noise ratio and visual noise of mobile phone cameras," *J. Imag. Sci. Technol.*, vol. 59, no. 1, 2015, Art. no. 10401.

[20] *EMVA Standard 1288–Standard for Characterization of Image Sensors and Cameras, Release 3.1*, European Machine Vision Association, Barcelona, Spain, 2016, pp. 18–20.

[21] *Canon EOS 800D Specifications*, Canon, Tokyo, Japan, 2017.

[22] J. McCann and A. Rizzi, "Optical veiling glare limitations to in-camera scene radiance measurements," in *Proc. Eur. Conf. Vis. Perception (ECVP)*, Sankt Peterburg, Russia, 2006, p. 5813.

[23] J. J. McCann and A. Rizzi, "Veiling glare: The dynamic range limit of HDR images," *Proc. SPIE*, vol. 6492, pp. 394–403, Feb. 2007.

[24] I. Tomić, I. Karlović, and I. Jurič, "Practical assessment of veiling glare in camera lens system," *J. Graph. Eng. Des*, vol. 5, no. 2, pp. 23–28, 2014.

[25] N. L. Koren, "Correcting misleading image quality measurements," *Electron. Imag.*, vol. 32, pp. 1–10, Jan. 2020.

[26] N. Koren, "Measuring the impact of flare light on dynamic range," *Electron. Imag.*, vol. 30, pp. 1–6, Jan. 2018.

[27] *About Libraw*, LibRaw, Potomac, MD, USA, 2008. Accessed: Feb. 16, 2023.

Alice Plutino received the Ph.D. degree from the Università degli Studi di Milano, Milan, Italy, in 2021.

She is currently an MSCA Post-Doctoral Fellow with the Faculty of Media Studies, University of Amsterdam, Amsterdam, The Netherlands, where she is also an Adjunct Professor with the Centro Sperimentale di Cinematografia, teaching digital film restoration and digital media conservation. She is the author of the book *Tecniche di Restauro Cinematografico* and several journals and conference papers of national and international relevance. Her research interests include color science, colorimetry, image enhancement, image digitization, and archiving, with a particular interest in cultural heritage applications.

Dr. Plutino is a member of the Italian Color Group (Gruppo del Colore), the Deputy Editor of the *Color Culture and Science Journal* (CCSJ), the Vice-Coordinator of Division One, and the Coordinator of Division Eight of NC CIE Italy. In 2023, she was awarded a Marie Skłodowska-Curie Postdoctoral Fellowship.

Michele Bagnati is currently an Electro-Acoustic Freelance Designer. His studies have focused on multimedia technical topics, such as signal analysis, coding, digital imaging, and electroacoustics. Add to that DIY maker skills for prototyping 3-D models and the consequent realization of them. He is an External Collaborator at MISP and LIM (research labs at Università degli Studi di Milano, Milan, Italy), continuing also with seminaries for students. His actual work is research development and testing acoustic loudspeakers with the consequent measure and data analysis.

Alessandro Rizzi is currently a Full Professor with the Department of Computer Science, University of Milano, Milan, Italy, where he teaches multimedia, colorimetry, and film restoration. He is the Head of the MIPS Laboratory, Department of Computer Science. Since 1990, he has been doing research in the field of digital imaging with a particular interest in color, visualization, photography, HDR, and the perceptual issues related to digital imaging, interfaces, and lighting.

Dr. Rizzi is a member of several program committees of conferences related to color and digital imaging. He has been one of the founders of the Italian Color Group, a Secretary of CIE Division Eight, an IS&T Fellow, and a Vice President. In 2015, he received the Davies Medal from the Royal Photographic Society. He is the Co-Chair of the IS&T Conference "Color Imaging: Displaying, Processing, Hardcopy and Applications," a Topical Editor of *Applied Color Science* of the *Journal of Optical Society of America A*. He is a Senior Editor of *Color Research and Applications* and an Associate Editor of the *Journal of Electronic Imaging*.